Supporting Information: Filterless Non-dispersive Infrared Sensing using Narrowband Infrared Emitting Metamaterials

Alyssa Livingood[1,2*], J. Ryan Nolen[3*], Thomas G. Folland[4,5], Lauren Potechin[4], Guanyu Lu[4], Scott Criswell[6], Jon-Paul Maria[7], Christopher T. Shelton[8], Edward Sachet[8], Joshua D. Caldwell[4]

1. Department of Electrical and Computer Engineering, University of Kentucky, Lexington, KY 40506, United States
2. Research Experience for Undergraduates (REU) program, Vanderbilt Institute for Nanoscale Science and Engineering (VINSE), Nashville, TN 37212, United States
3. Interdisciplinary Materials Science Program, Vanderbilt University, Nashville, TN 37212, United States
4. Department of Mechanical Engineering, Vanderbilt University, Nashville, TN 37212, United States
5. Department of Physics and Astronomy, The University of Iowa, IA, 52242, United States
6. Department of Electrical Engineering, Vanderbilt University, Nashville, TN 37212, United States
7. The Pennsylvania State University, State College, PA 16801, United States
8. Third Floor Materials, Raleigh, NC 27695, United States

* Equal contributions

9 pages, 8 figures

I. Polarization Dependent Thermal Emission Measurements

As was stated in the main text, cadmium oxide (CdO) films of deeply subwavelength thicknesses support both Berreman and epsilon-near-zero (ENZ) modes where $Re[\varepsilon_{CdO}(\omega)] \approx 0$. In planar films on an unstructured substrate (Fig. S1e) Berreman and ENZ modes can only be supported in *p*-polarization, with the former being accessible from free space. Reciprocally, through Kirchhoff's law, only *p*-polarized thermal emission is expected to be generated from CdO planar films through the thermal excitation of the Berreman mode. Since the Berreman mode is unable to couple to *s*-polarized emission, the maximum unpolarized thermal emission that can be harnessed from the sample is limited to 50%. However, by depositing an identical CdO film on a patterned sapphire substrate (PSS), as we have done here (Fig. S1F), the momentum mismatch between free space light and the ENZ polariton mode can bridged, enabling both *s*- and *p*-polarizations to be absorbed/emitted. It is important to reiterate that in the flat CdO film that only the Berreman mode can be accessed from free space, whereas the ENZ mode can be coupled from free space only if the wavevector of the incident light can be increased as is observed in the CdO films grown on the PSS, giving rise to our nanophotonic infrared emitting metamaterial (NIREM) samples. The dispersion relation for these excitations is discussed later in section III of the supporting information. Therefore, the total emissivity of the PSS sample can in principle reach a value of 1, in contrast to the 0.5 limit appropriate for the flat film.

In order to confirm the polarization response of the flat and PSS CdO emitters, we performed polarized, angle-dependent thermal emission measurements of a 120 nm CdO film ($N_d = 5.8\ x\ 10^{19}\ cm^{-3}$) deposited onto a flat, Au-coated (110 nm) sapphire substrate (Fig. S1a and S1c) and a PSS also featuring the same thickness Au film (Fig. S1b and S1d). These measurements are detailed in the methods section and a schematic of the beam path is provided in Fig. S7. The unpolarized thermal emission from these samples are provided in Fig. 2 and 3 of the main text. The thermal emission from the flat film exhibits a significant polarization dependence as expected. In *p*-polarization (Fig. S1c), the thermal emissivity climbs from $\epsilon \approx 0$ to nearly $\epsilon \approx 0.8$ ($\epsilon \approx 0.4$ for unpolarized measurements) at the plasma frequency as the angle of emission is increased from 0˚ to 80˚, with the strongest emission occurring near 70°. However, in *s*-polarization (Fig. S1a) the emissivity remains consistently-low and featureless, even as the emission angle is increased. In contrast, the CdO-coated PSS sample is strongly emissive for both polarizations, with the emission peaking at the ENZ frequency ($\omega_{ENZ} \approx 2550\ cm^{-1}$) in both in both *s*- and *p*-polarization. Further, the radiation pattern is completely changed, with the thermal emission most strongly observed at angles between 0° (normal to sample surface) and 40°. This is due to the symmetry of the PSS pattern, which allows the ENZ mode to be out-coupled in both polarizations. Further, the dispersive, diffractive resonance present in the unpolarized measurements (Fig. 2 and 3) is evident in both polarizations as well.

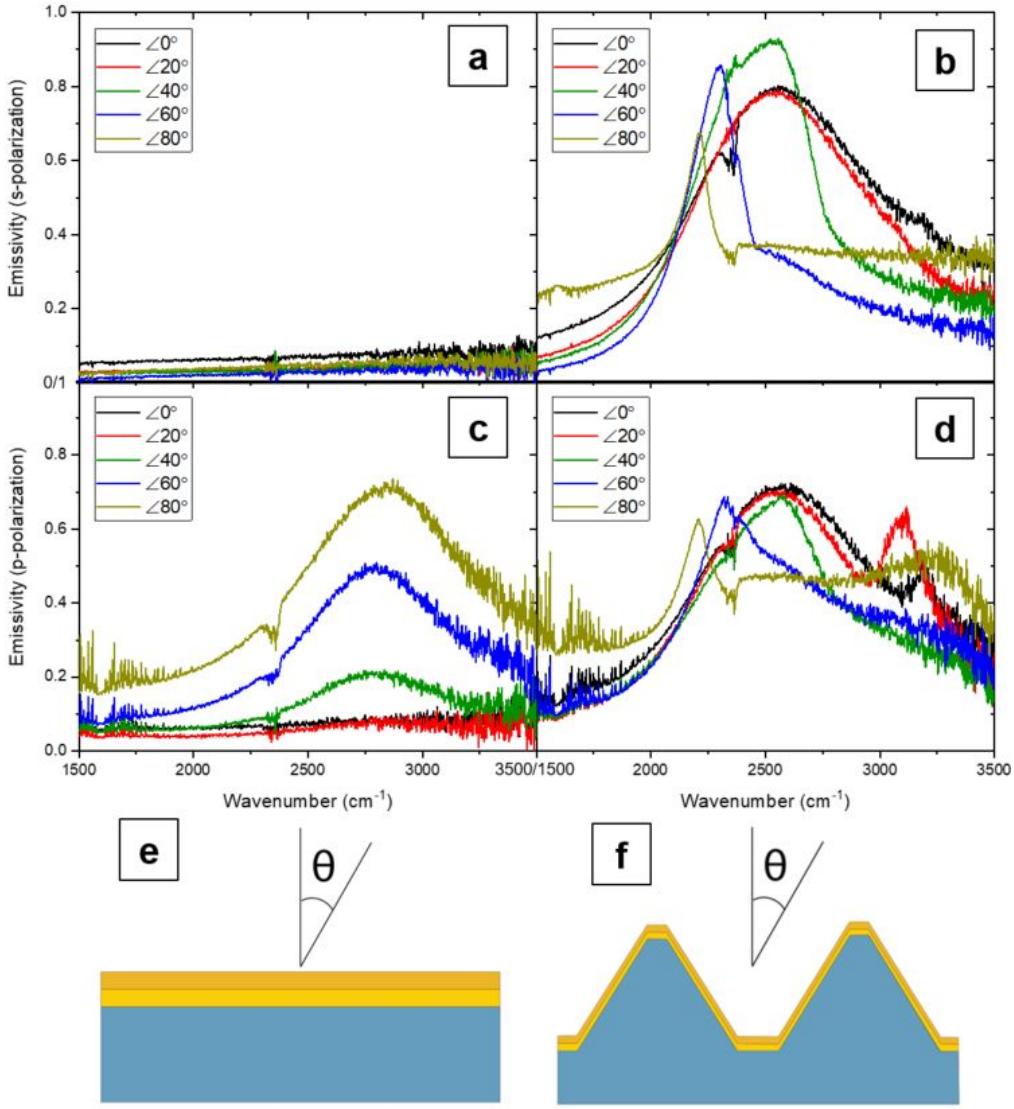

Figure S1: *(a) and (c) show the s- and p-polarized thermal emission from the CdO on PSS sample depicted in (e). (b) and (d) show the s- and p-polarized thermal emission spectra for the CdO flat film sample depicted in (f).*

II. Patterned Sapphire Substrate Pitch Dependence

Due to the wavelength-scale pitch ($p = 3.02\ \mu m$) of the PSS structure, the thermal emission spectra exhibit a highly dispersive mode that we attribute to the excitation of a diffractive order. We justify this by examining the E_z and $\vec{S}$ profiles, which are provided in Fig. 4b. Here we provide additional justification through simulation results illustrating the pitch-dependence of the spectral position for this dispersive mode. Due to the hexagonal pattern of the PSS, approximating the system as a simple 1D grating does not fully reproduce the spectral position of the diffractive mode. Instead, the PSS must be viewed as a 2D photonic crystal with the diffractive order corresponding to the lowest energy mode lying within the free-space light cone of the photonic dispersion.

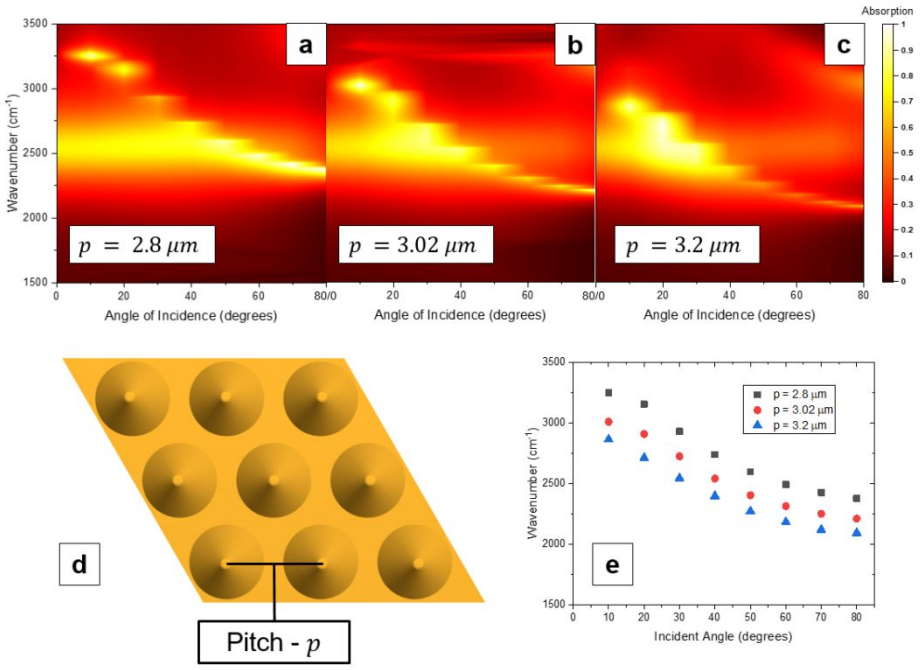

Figure S2: *Contour plots displaying the simulated angle-dependent p-polarized absorption for (a) $p = 2.8\ \mu m$, (b) $p = 3.02\ \mu m$, and (c) $p = 3.2\ \mu m$. (d) Topview of CdO on PSS sample with pitch labeled. (e) Spectral dispersion of diffractive mode for three pitches shown in (a), (b), and (c).*

Using CST studio suite, we performed numerical calculations (Fig. S2) of the *p*-polarized, angle-dependent absorption for CdO on PSS structures featuring three pitches ($p = 2.8,\ 3.02$ and $3.2\ \mu m$). In these simulations, the base diameter ($b = 2.4\ \mu m$) and height of the cones ($h = 1.58\ \mu m$), as well as the Au and CdO layer thicknesses remained constant. Additional details about these simulations are provided in the methods section. For all three pitches, in addition to the ENZ absorption centered at $\omega_{ENZ} \approx 2550\ cm^{-1}$, there is a diffractive resonance that tunes towards lower frequencies with increased angle of incidence. For clarity, we provide the spectral position of this diffractive mode alone, in Fig. S2e, revealing a clear spectral dependence on the PSS pitch. Namely, a decrease (increase) in the PSS pitch results in a blueshift (redshift) in the spectral location of the diffractive mode. Alternatively, at the same frequency (ω) the diffractive mode is shifted to higher in-plane momentum (larger incident angle) as the pitch decreases. This is consistent with diffractive coupling using a grating, wherein the additional in-plane momentum provided by the grating is inversely dependent on the pitch ($G = 2\pi/p$).

The measured, angle-dependent thermal emission of the fabricated CdO PSS (Fig. 2 and 3) shows that the diffractive mode for $p = 3.02\ \mu m$ originates (Γ-point, 0˚) at a frequency greater than the ENZ frequency and tunes through the ENZ mode at higher emission angles. The spectral overlap of the modes results in an interference effect that significantly decreases the emission linewidth. From the simulation results provided in Fig. S2, we have determined that the spectral position at a given angle redshifts as the pitch increases. Therefore, it is conceivable that by increasing the PSS pitch such that the diffractive mode at the Γ-point overlaps with the ENZ emission, that this interference effect and spectral narrowing could in principle be realized at 0˚. Indeed, simulation results reveal (Fig. S3) that a significant narrowing of the absorption linewidth can potentially be achieved at normal incidence by increasing the PSS pitch to $p = 5\ \mu m$.

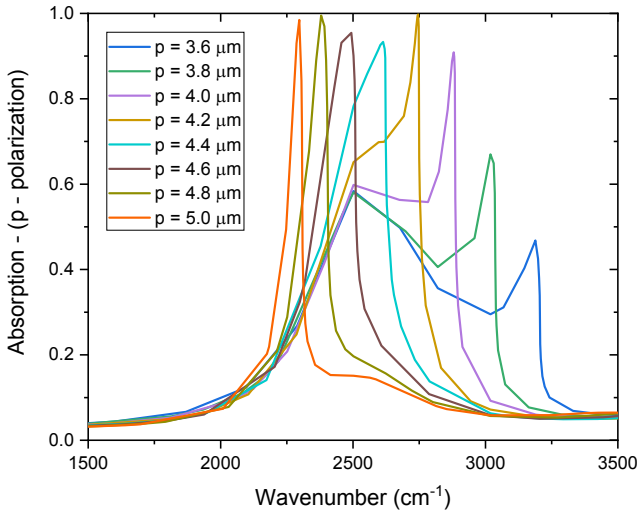

Figure S3: *Simulated p-polarized absorption spectra detailing the pitch dependence at normal incidence for the CdO on PSS sample. As the pitch is increased and diffractive mode redshifts through the ENZ mode, the interference effect leads to a reduction in absorption linewidth.*

III. Dispersion Relation of Berreman and Epsilon-Near-Zero Modes

Berreman and ENZ modes are both supported in CdO thin films and are spectrally located at the zero-crossing of the real permittivity $Re[\varepsilon_{CdO}(\omega)] \approx 0$, however, they lie on opposite sides of the free-space light line. The dispersion relationship of Berreman and ENZ modes supported in a thin films can be calculated by considering a thin film (ε_2) separating two semi-infinite dielectric media (ε_1 - top, ε_3 - bottom) illuminated under *p*-polarization.[1]

$$1 + \frac{\varepsilon_1 k_{z3}}{\varepsilon_3 k_{z1}} = i\tan(k_{z2}d)\left(\frac{\varepsilon_2 k_{z3}}{\varepsilon_3 k_{z2}} + \frac{\varepsilon_1 k_{z2}}{\varepsilon_2 k_{z1}}\right) \qquad (1)$$

In eqn. 1, ε_i is the complex dielectric function, d is the film thickness, and $k_{zi}^2 = \varepsilon_i \frac{\omega^2}{c^2} - k_{\parallel}^2$ where $i = 1, 2, 3$. Using the transfer matrix method (TMM) we calculated the full dispersion of the CdO flat film in this study ($d = 120\ nm$, $N_d = 5.8\ x\ 10^{19}\ cm^{-3}$) with in-plane wavenumber $k_{\parallel}$ spanning from below to above the free-space light line (Fig. S4). The Berreman mode exists within the light line and therefore can couple directly to free-space, even in flat films. Thus, it is the Berreman mode that is responsible for the thermal emission from the CdO flat film sample and not the ENZ mode, for which the dispersion exists outside of the free space light line and therefore requires additional momentum in order to be excited.[1,2] There is also a clear blueshift in the spectral position as the Berreman mode approaches the light line (at steep angles of incidence/emission). This explains the slight blue shift observed in the thermal emission spectra (Fig. 2 and S1c) of the CdO flat film. Conversely, the CdO PSS NIREM is capable of also out-coupling the emission from the thermally-excited ENZ mode to free-space, even at normal incidence. This is a result of scattering from the conical structures that provide the auxiliary momentum necessary to couple to the ENZ mode. As opposed to the Berreman mode, the ENZ mode shows little spectral dispersion with incident/emission angle and therefore there is little dependence on the spectral position of the ENZ emission with emission angle from the CdO NIREM (Fig. 2b and 2d), with the obvious exception of the diffraction induced interference effects as described above.

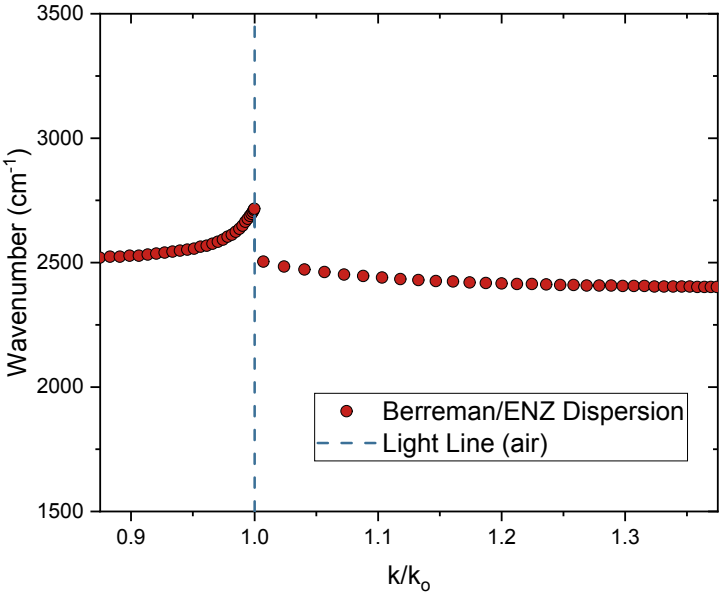

Figure S4: *Berreman/epsilon-near-zero dispersion calculated using TMM[3] of a 120 nm thick CdO film. As the Berreman mode approaches the light line from the left, a blue shift is observed. This explains the slight blue shift at highly off-normal angles (80˚) in the thermal emission spectra from the flat film samples (Fig. 2a of the text, and S1d).*

IV. Spectral Bandwidth of CdO NIREM Source

Although our device is successful in detecting trace concentrations of CO_2, we would like to point out that the emission linewidth of the CdO NIREM does not only overlap with this molecular absorption, but also with absorption peaks associated with other common gasses, such as CO and N_2O (Fig. S5). As was state in the text, CdO ENZ absorber/emitter linewidths have been reported to be as low as 307 cm^{-1}[4] so the device reported here does not represent the narrowest possible absorption/emission linewidth. From the SEM images collected of the CdO NIREM on PSS devices, the top surface of the films appears rough, presumably resulting in significant increases in scattering-based losses, thereby broadening the linewidth with respect to prior state-of-the-art. Similar surface roughness is also observed in CdO grown on metallic films such as Au (Fig. S6b), as this results in a columnar growth (Fig. S6f). Thus, one alternative approach would be to replace the metallic film with a CdO layer with carrier density well in excess of the CdO ENZ emitting layer. As the plasma frequency of such a highly doped layer will be well in excess of the emitting layer, this would serve the same highly reflective role

that the metal layer currently serves. As such columnar growth is not observed in growth on sapphire or CdO, the losses would be anticipated to be significantly reduced. Another approach is through optimizing the PSS periodicity, as is described in section II, whereby further narrowing of the emission linewidth at normal incidence could also be potentially achieved. In this optimized geometry the spectral overlap with non-targeted molecular absorption bands would no longer be present.

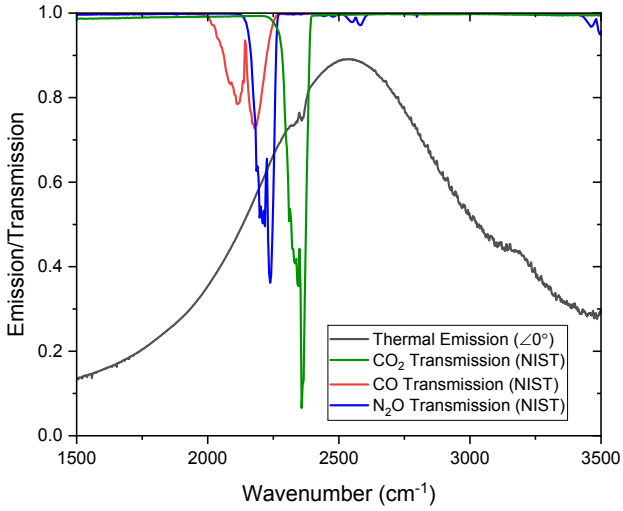

Figure S5: *Normal (0˚) incidence thermal emission from CdO on PSS sample, showing spectral overlap with CO_2, N_2O, and CO absorption.*[5]

V. Scanning Electron Microscope Images of NIREM Device

We collected SEM images of the CdO PSS emitter using a Zeiss Merlin SEM in order to determine the geometry of the hexagonal lattice and conical structures (Fig. S6). This also allowed us to determine the alignment of the hexagonal lattice with respect to the overall sample in order to align the polar angle along the $[11\bar{2}0]$ axis during angle-dependent thermal emission measurements.

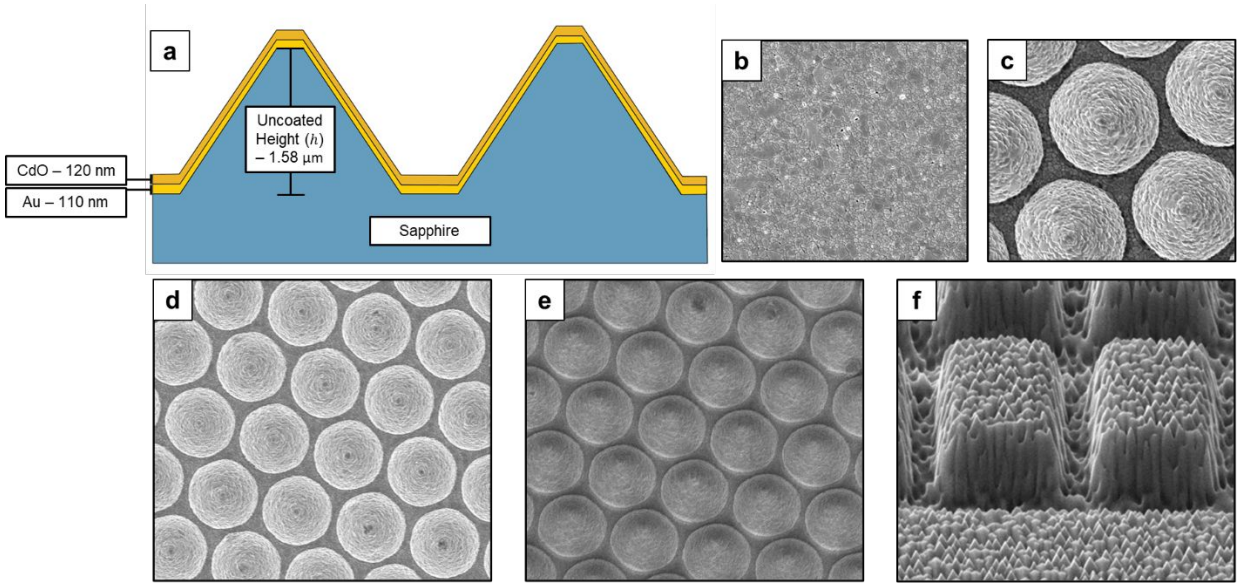

Figure S6: *(a) Schematic of cut of showing cone height and layer thicknesses. (b) SEM image of the CdO-coated flat substrate sample. SEM images of coated CdO on PSS samples at (d) normal incidence and (e) 22˚ angle of incidence. In (f) we provide an SEM image of a milled CdO film grown on a metal backplane in order to show the columnar growth.*

VI. Beam Diagram of Thermal Emission and Gas Cell Measurements

Here we provide the beam profiles for the angle-dependent thermal emission measurements (Fig. S7a) and the CO_2 transmission measurements (Fig. S7b). The procedure for both of these measurements is provided in the methods section.

VII. Error Analysis of CO_2 Detection

Using the procedure provided in the methods section, ten CO_2 transmission measurements were performed in succession using our CdO NIREM at CO_2 concentrations of 100 ppm and 200 ppm. From each set of measurements, we were then able to calculate the average CO_2 absorption and standard deviation at each concentration. This allowed us to determine the influence of ambient CO_2 and temperature fluctuations on the CO_2 transmission measurements. The average in the standard deviation within the CO_2 absorption band (~2325 – 2375 cm^{-1}) was calculated to be 0.09 and 0.11 for 100 ppm and 200 ppm, respectively. Therefore, the noise floor due to temperature and CO_2 fluctuations remains consistent for both concentrations. If we were to increase the number of measurements used in our error analysis we believe that the average standard deviation values for each concentration would converge.

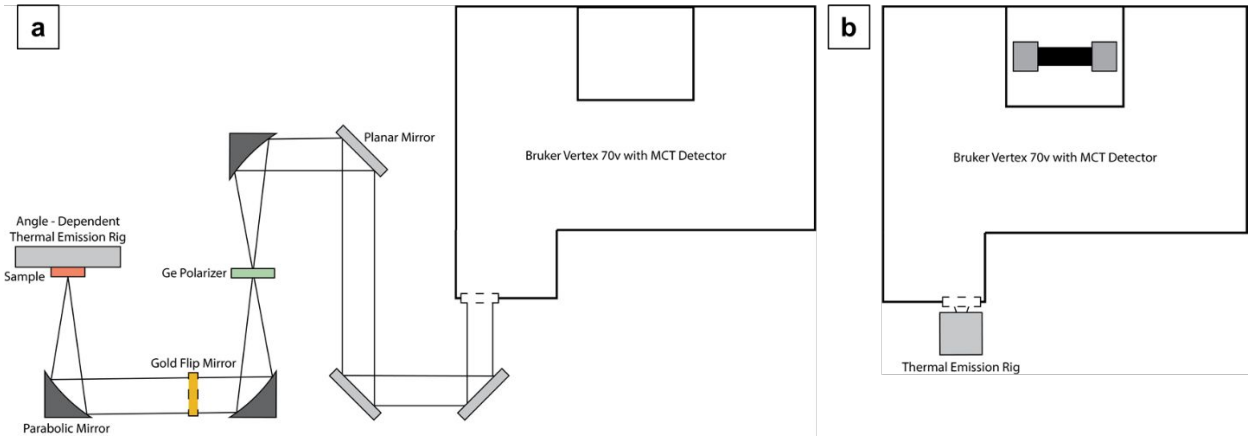

Figure S7: *(a) Experimental setup showing external, angle-dependent thermal emission rig. (b) Backport for angular rig as well as external backport thermal emission device used for gas cell measurements. Both diagrams are not drawn to scale.*

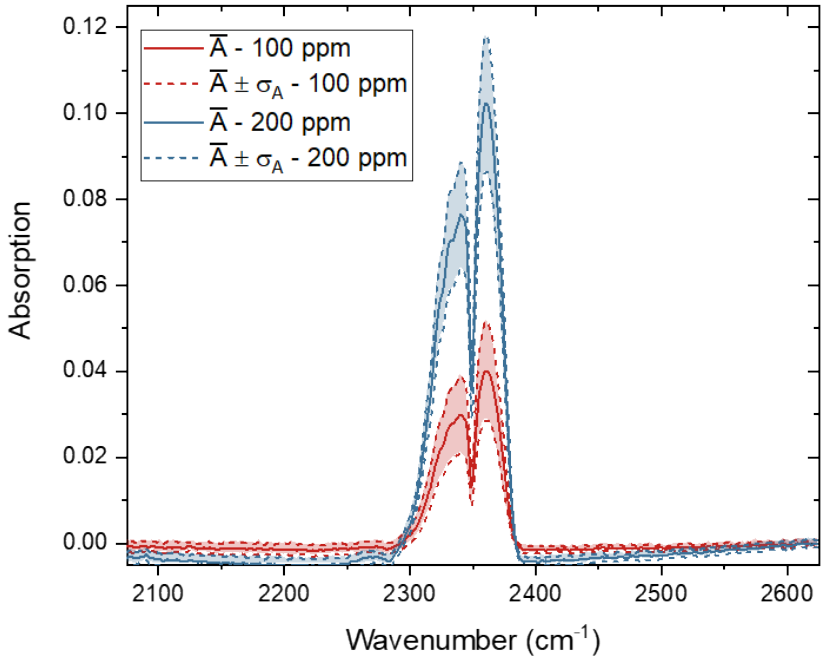

Figure S8: *Absorption spectra illustrating the error analysis performed at CO_2 concentrations of 100 ppm and 200 ppm for our CdO NIREM. The solid lines show the average ($\bar{A}$) of 10 absorption spectra performed at 250°C. The dashed lines show the average shifted by the standard deviation (σ_A).*

References

(1) Vassant, S.; Hugonin, J.-P.; Marquier, F.; Greffet, J.-J. Berreman Mode and Epsilon near Zero Mode. *Opt. Express* **2012**, *20* (21), 23971–23977.

(2) Campione, S.; Brener, I.; Marquier, F. Theory of Epsilon-near-Zero Modes in Ultrathin Films. *Phys. Rev. B* **2015**, *91*, 121408. https://doi.org/10.1103/PhysRevB.91.121408.

(3) Passler, N. C.; Paarmann, A. Generalized 4 × 4 Matrix Formalism for Light Propagation in Anisotropic Stratified Media: Study of Surface Phonon Polaritons in Polar Dielectric Heterostructures. *J. Opt. Soc. Am. B* **2017**, *34* (10), 2128–2139. https://doi.org/10.1364/josab.34.002128.

(4) Kelley, K. P.; Runnerstrom, E. L.; Sachet, E.; Shelton, C. T.; Grimley, E. D.; Klump, A.; Lebeau, J. M.; Sitar, Z.; Suen, J. Y.; Padilla, W. J.; Maria, J.-P. Multiple Epsilon-Near-Zero Resonances in Multilayered Cadmium Oxide: Designing Metamaterial-Like Optical Properties in Monolithic Materials. *ACS Photonics* **2019**, *6* (5), 1139–1145. https://doi.org/10.1021/acsphotonics.9b00367.

(5) Linstrom, P. J.; Mallard, W. G.; (eds.). *NIST Chemistry WebBook, NIST Standard Reference Database Number 69*; National Institute of Standards and Technology: Gaithersburg MD.